Backward saturation in four-wave mixing in neon: Case of parallel pump polarizations

P. Verkerk, M. Pinard, and G. Grynberg
Laboratoire de Spectroscopie Hertzienne de l'Ecole Normale Supérieure, Université Pierre et Marie Curie, 75252 Paris Cédex 05, France
(Received 9 June 1986)

We present in this paper a theoretical and experimental study of the effect of an intense pump beam on four-wave-mixing emission in the geometry of phase conjugation. The theoretical model is developed for Γ (natural width) $< \Omega_1$ (Rabi frequency of the intense pump) $< ku$ (Doppler width) and uses the dressed-atom approach. We have analyzed degenerate and nearly degenerate four-wave mixing. In this latter case, we have studied three situations according to which beam (intense pump, weak pump, or probe) has a different frequency. The experimental study has been done in a neon cell using cw lasers. Our experimental results are in excellent agreement with theory. This study shows the need to take into account the atomic motion in the theory. However a quantitative analysis cannot be done assuming an infinite Doppler width and we show the importance of the Boltzmann factor. In the case of nearly degenerate four-wave mixing, narrow resonances corresponding to transitions between energy levels of the dressed atom are observed.

I. INTRODUCTION

Degenerate and nearly degenerate four-wave mixing has been extensively studied during the recent years.[1] One reason for this interest is the possibility of obtaining efficient phase conjugation using four-wave mixing.[2] For instance, phase-conjugate reflectivities higher than one have been obtained in atomic sodium vapor[3] and have opened the possibility of observing self-oscillation in cavities closed by a sodium-vapor phase-conjugate mirror.[4] However, the understanding of four-wave mixing in atomic vapors has for a long time been restricted to the perturbative limit.[5] Saturation effects were generally described with motionless-atom models.[6] When the Rabi frequency Ω_1 is smaller than the Doppler width these theories give incorrect predictions as shown by Bloch *et al.*[7] More precisely, these authors consider the case of one saturating pump beam and one weak pump beam. They show that the intensity of the phase-conjugate beam is larger in the case of backward saturation (intense pump beam and probe beam propagating in opposite directions) than in the case of forward saturation (intense pump beam and probe beam propagating in the same direction). This result cannot be interpreted by a motionless-atom model. Soon after, Bloch and Ducloy[8] presented a semiclassical theory of the effect of one saturating pump beam in degenerate four-wave mixing in a Doppler-broadened medium. We have afterwards presented a simpler approach using the dressed-atom model.[9] The main advantage of this theory is that it considerably clarifies the underlying physics and it leads to simple physical pictures. In the case of backward saturation we have shown that the signal is generated by two velocity groups only. For these velocity groups the Doppler effect tunes the incident frequencies to obtain a resonant nondegenerate four-wave-mixing emission on a Rabi sideband, in the atomic frame. (The enhancement of four-wave-mixing emission on a Rabi sideband in the nearly degenerate case was previously considered by Harter and Boyd in the case of stationary atoms.[10] It is interesting to notice that this effect permits us to understand the saturation effects in the degenerate case for a Doppler-broadened medium.)

In our preceding papers[9,11] we have considered the case of a resonance line and we have calculated the line shape for a two-level atom in the backward-saturation and forward-saturation cases. We have also analyzed the effect of collisional damping and the situation where the weak pump beam can also saturate the atomic transition. In the present paper, we adapt the theoretical model to the experimentally studied situation of a transition between two excited levels. We calculate the line shape in degenerate four-wave mixing in the case of backward saturation. We discuss the influence of the Doppler width and of the distribution of intensity in a realistic Gaussian beam. Afterwards, we extend our calculations to the case of nearly degenerate four-wave mixing in two-level atoms. We consider two incident beams of frequency ω_L and the third incident beam of frequency ω_L'. We show that the line shapes are strongly different according to which beam (intense pump, weak pump, or probe) has a different frequency. We then present experimental results obtained in a neon discharge in the case of three incident beams of the same polarization. In the degenerate case we show that an excellent quantitative agreement is obtained between experiment and theory when the effect of finite Doppler width is taken into account. In the nearly degenerate case we also obtain very good agreement with theoretical predictions. In particular, we have observed narrow resonances which are located on the Rabi sidebands. These resonances correspond to a Doppler-free spectrum of atoms dressed by the saturating optical field. The good agreement obtained in all the experimental situations that we have considered demonstrates the validity of our theoretical method and shows that the problem of one-

beam saturation in degenerate and nearly degenerate four-wave mixing in atomic vapors seems now to be fully understood.

II. THEORY: THE DRESSED-ATOM MODEL

A. General description

We consider three electromagnetic waves $\mathbf{E}_1$, $\mathbf{E}_2$, and $\mathbf{E}_3$ whose frequencies are ω_L, ω_L', and ω_L'' and whose wave vectors are $\mathbf{k}_1$, $\mathbf{k}_2$, and $\mathbf{k}_3$ [Fig. 1(a)]. The pump beams $\mathbf{E}_1$ and $\mathbf{E}_2$ propagate in opposite directions ($\mathbf{k}_1/|k_1| = -\mathbf{k}_2/|k_2|$). The z axis is parallel to $\mathbf{k}_2$. The three waves have the same linear polarization ε. We assume that the frequencies of the incident waves are close to the resonance frequency ω_0 of a two-level atom [Fig. 1(b)]. We suppose that $|a\rangle$ and $|b\rangle$ are two excited levels which are populated in a discharge with a rate Λ_a and Λ_b. We take a single relaxation constant Γ for the populations of $|a\rangle$ and $|b\rangle$ and for the atomic coherence.

We assume that the only wave which saturates the atomic transition is $\mathbf{E}_1$. Its amplitude $|\mathbf{E}_1|$ is sufficiently large to obtain a Rabi frequency $\Omega_1 = d|\mathbf{E}_1|/\hbar$ larger than Γ (d is the matrix element of the electric dipole moment between $|a\rangle$ and $|b\rangle$). On the other hand, Ω_1 is smaller than the Doppler width ku of the a-b transition. The other waves $\mathbf{E}_2$ and $\mathbf{E}_3$ have a much weaker amplitude, the corresponding Rabi frequencies Ω_2 and Ω_3 being smaller than Γ. The assumption of our theoretical development is thus

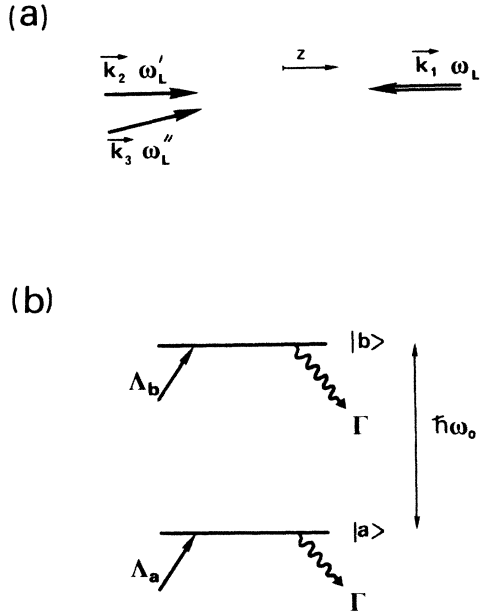

FIG. 1. (a) Scheme of the incident beams in the four-wave mixing geometries studied in the paper. The two pump beams $\mathbf{E}_1$ and $\mathbf{E}_2$ propagate in opposite directions, the probe beam makes a very small angle θ with the pump-beam direction. The three beams have the same linear polarization. (b) The two-level-atom model considered in this paper. The pumping rates are Λ_a and Λ_b. We assume that the two levels have the same lifetime ($1/\Gamma$).

$$\Omega_2, \Omega_3 < \Gamma \ll \Omega_1 < ku \ . \tag{1}$$

We study here the case where the probe beam $\mathbf{E}_3$ propagates in a direction opposite to the intense-pump beam $\mathbf{E}_1$ [see Fig. 1(a)]. This is the backward saturation case. The situation where $\mathbf{E}_3$ and $\mathbf{E}_1$ are almost colinear (forward saturation) corresponds to a weaker phase-conjugate efficiency and is not treated here. The line shape in forward saturation for a two-level atom has already been calculated in the case of Fig. 1(b) in Ref. 12 and for a resonance line in Ref. 11.

The component of the electric dipole moment which radiates the phase-conjugate beam is calculated in the atomic rest frame. The wave frequencies are Doppler shifted in this frame. For an atom of velocity v_z, the frequencies of the three incident beams become

$$\omega_1 = \omega_L(1+v_z/c) \ , \tag{2a}$$

$$\omega_2 = \omega_L'(1-v_z/c) \ , \tag{2b}$$

$$\omega_3 = \omega_L''(1-v_z/c) \ . \tag{2c}$$

Note that we have assumed a very small angle θ between the directions of propagation of $\mathbf{E}_2$ and $\mathbf{E}_3$ in order to obtain a residual Doppler width ($\sim k\theta u$) small compared to Γ.

In the following we make a quantum treatment of the intense wave $\mathbf{E}_1$ and a classical treatment of the weak waves $\mathbf{E}_2$ and $\mathbf{E}_3$. We shall thus consider the interaction of a two-level atom dressed by an intense optical field[13] with two weak classical fields. We first apply this model to calculate the electric dipole moment for a velocity group v_z. The calculated value is then averaged over the velocity distribution. We finally assume that the medium is optically thin, i.e., that the three incident waves are very slightly modified during their propagation. The theoretical variation of the generated beam intensity which is obtained is compared with experimental results in Sec. III.

B. Mean value of the electric dipole moment for a velocity group v_z

We have assumed that Ω_2/Γ and Ω_3/Γ are small compared to 1. We can thus make a perturbation expansion in power of Ω_2/Γ and Ω_3/Γ of the density matrix of the dressed atom. At the lowest order, the amplitude of the dipole which radiates the phase-conjugate beam is proportional to $\Omega_2\Omega_3$. We must thus calculate the density matrix to second order in the weak fields $\mathbf{E}_2$ and $\mathbf{E}_3$. On the other hand, we exactly describe the effect of $\mathbf{E}_1$. As a first step, we shall consider the density matrix of the atom dressed by the photons of the intense beam $\mathbf{E}_1$ and we will afterwards treat the effect of $\mathbf{E}_2$ and $\mathbf{E}_3$ using a perturbation method.

1. The density matrix of the dressed atom to zeroth order in the weak fields

In this section we consider the interaction of the atoms with the intense wave $\mathbf{E}_1$. At the rotating-wave approximation, the Hamiltonian of the dressed atom in the laboratory frame is equal to

$$H_0=\hbar\omega_0\,|\,b\rangle\langle b\,|+\hbar\omega_L a^\dagger a$$
$$-\mathscr{E}d(D_+ae^{i\mathbf{k}_1\cdot\mathbf{r}}+D_-a^\dagger e^{-i\mathbf{k}_1\cdot\mathbf{r}}) \quad (3)$$

with $D_+=|\,b\rangle\langle a\,|$. a and $a^\dagger$ are the annihilation and creation operators of a photon in the mode $(\mathbf{k}_1,\boldsymbol{\varepsilon})$. $\mathscr{E}$ is a coupling constant.

In order to obtain the Hamiltonian in the atomic rest frame, we make the following unitarity transformation:[11]

$$T=\exp[ia^\dagger a(\mathbf{k}_1\cdot\mathbf{r})]\,, \quad (4)$$

where $\mathbf{r}$ corresponds to the atomic motion

$$\mathbf{r}=\mathbf{r}_0+\mathbf{v}t\,. \quad (5)$$

Using (3)–(5), we obtain the Hamiltonian in the atomic frame,

$$H_T=TH_0T^\dagger+i\hbar\frac{\partial T}{\partial t}T^\dagger$$
$$=\hbar\omega_0\,|\,b\rangle\langle b\,|+\hbar\omega_1a^\dagger a-\mathscr{E}d(D_+a+D_-a^\dagger)\,, \quad (6)$$

where ω_1 is the Doppler-shifted frequency (2a). The field is described by a Glauber coherent state. In the laboratory frame at $t=0$, this state is $|\,\alpha\rangle$ (where $\alpha=|\,\alpha\,|e^{i\theta_1}$). At time t, in the atomic frame, the state of the field is

$$|\,\alpha_T(t)\rangle=T\,|\,\alpha(t)\rangle\,,$$
$$|\,\alpha_T(t)\rangle=e^{-|\alpha|^2/2}\sum_n\frac{|\,\alpha\,|^n}{\sqrt{n!}}e^{-in(\omega_1t+\phi_1)}\,|\,n\rangle\,, \quad (7)$$

where

$$\phi_1=-(\mathbf{k}_1\cdot\mathbf{r}_0+\theta_1)\,. \quad (8)$$

The average value of the number of photons in this state is $\bar{n}=|\,\alpha\,|^2$ and the resonance Rabi notation frequency Ω_1 is equal to[13]

$$\Omega_1=-2\left[\frac{\mathscr{E}d}{\hbar}\right]\sqrt{\bar{n}}\,. \quad (9)$$

The eigenstates $|\,i,n\rangle$ of H_T are

$$|\,i,n\rangle=\alpha_i\,|\,a,n+1\rangle+\beta_i\,|\,b,n\rangle\quad(i=1,2) \quad (10a)$$

with

$$\alpha_1=-\beta_2=\sin\varphi\,, \quad (10b)$$

$$\beta_1=\alpha_2=\cos\varphi\,, \quad (10c)$$

the angle φ being defined by

$$\tan(2\varphi)=\frac{\Omega_1}{\omega_0-\omega_1}=\frac{\Omega_1}{\delta_1}\,, \quad (11)$$

where we have introduced the frequency detuning $\delta_1=\omega_0-\omega_1$.

The corresponding energies are

$$E_{i,n}=(n+1)\hbar\omega_1+E_i \quad (12)$$

with

$$E_1=\tfrac{1}{2}\hbar(\delta_1+\bar{\Omega})\,, \quad (13a)$$

$$E_2=\tfrac{1}{2}\hbar(\delta_1-\bar{\Omega})\,, \quad (13b)$$

where $\bar{\Omega}$ is the Rabi frequency

$$\bar{\Omega}=(\delta_1^2+\Omega_1^2)^{1/2}\,. \quad (14)$$

The energy diagram of the dressed atom is shown in Fig. 2. It consists of a ladder of doublets separated by $\hbar\omega_1$. The distance between two levels of the doublet $\hbar\bar{\Omega}$ is assumed to be very small compared to $\hbar\omega_1$.

To zeroth order in the weak field, the master equation for the density matrix ${}_0\sigma$ of the dressed atom is

$$\frac{d}{dt}({}_0\sigma)=\frac{1}{i\hbar}[H_T,{}_0\sigma]+\left[\frac{d_0\sigma}{dt}\right]_{\rm rel}\,. \quad (15)$$

The pumping and the relaxation of the bare atom [Fig. 1(b)] are described by the equation

$$\left[\frac{d\rho}{dt}\right]_{\rm rel}=-\Gamma\rho+\Lambda\,, \quad (16)$$

where Λ is a diagonal matrix

$$\Lambda=\begin{bmatrix}\Lambda_b & 0\\ 0 & \Lambda_a\end{bmatrix}\,. \quad (17)$$

If we assume that $\bar{\Omega}$ is small compared to the inverse of the correlation time of creation and destruction of atoms in these levels, the master equation for ${}_0\sigma$ is

$$\frac{d({}_0\sigma)}{dt}=-\frac{i}{\hbar}[H_T,{}_0\sigma]-\Gamma({}_0\sigma)+\Lambda\otimes\rho_R(t)\,, \quad (18)$$

where $\rho_R(t)$ is the density matrix of the intense wave $\mathbf{E}_1$ $[\rho_R(t)=|\,\alpha_T(t)\rangle\langle\alpha_T(t)\,|\,]$. The matrix elements of ${}_0\sigma$ in the $|\,i,n\rangle$ basis (10) are

$${}_0\sigma^P_{ijn}=\langle i,n\,|\,{}_0\sigma\,|\,j,n-p\rangle \quad (19)$$

and the evolution of these matrix elements is deduced from (18),

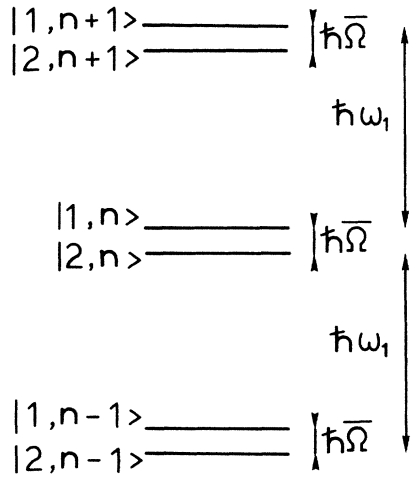

FIG. 2. Energy diagram of the dressed atom.

$$\frac{d({}_0\sigma^p_{jkn})}{dt}=-i\left[\frac{E_j-E_k}{\hbar}+p\omega_1\right]{}_0\sigma^p_{jkn}-\Gamma({}_0\sigma^p_{jkn})+\Lambda^p_{jkn} \tag{20}$$

with

$$\Lambda^p_{jkn}=\langle j,n\mid\Lambda\otimes\rho_R(t)\mid k,n-p\rangle\ . \tag{21}$$

Using (21) and (7) we find that Λ^p_{jkn} is proportional to $\exp[-ip(\omega_1 t+\phi_1)]$. In the following we shall consider the variation of the atomic variables, we are thus not interested in the information related to the index n of σ^p_{ijn}. Using the two preceding properties, we define

$$\tilde{\Lambda}_{jk}=e^{ip(\omega_1 t+\phi_1)}\sum_n\Lambda^p_{jkn}\ , \tag{22a}$$

$${}_0\tilde{\sigma}_{jk}=e^{ip(\omega_1 t+\phi_1)}\sum_n{}_0\sigma^p_{jkn}\ . \tag{22b}$$

We deduce from (20) the following equation for ${}_0\tilde{\sigma}_{jk}$:

$$\frac{d}{dt}{}_0\tilde{\sigma}_{jk}=-\frac{i}{\hbar}(E_j-E_k){}_0\tilde{\sigma}_{jk}-\Gamma({}_0\tilde{\sigma}_{jk})+\tilde{\Lambda}_{jk}\ . \tag{23}$$

We only consider the stationary solution of (23). The value of $\tilde{\Lambda}_{jk}$ is easily deduced from (7), (10), (17), and (21),

$$\tilde{\Lambda}_{jk}=\alpha_j\alpha_k\Lambda_a+\beta_j\beta_k\Lambda_b \tag{24}$$

and we find that ${}_0\tilde{\sigma}_{jk}$ is equal to

$${}_0\tilde{\sigma}_{jk}=\frac{\tilde{\Lambda}_{jk}}{i\dfrac{(E_j-E_k)}{\hbar}+\Gamma}\ . \tag{25}$$

The condition (1) implies that $\bar{\Omega}\gg\Gamma$. Using (13), we then deduce from (25) that the coherences ${}_0\tilde{\sigma}_{12}$ and ${}_0\tilde{\sigma}_{21}$ are very small compared to the populations ${}_0\tilde{\sigma}_{11}$ and ${}_0\tilde{\sigma}_{22}$. We can thus neglect the coherences (secular approximation) and we obtain for the stationary solution ${}_0\tilde{\sigma}_{ii}=\Pi_i$ with

$$\Pi_i=\frac{\tilde{\Lambda}_{ii}}{\Gamma} \tag{26}$$

and ${}_0\tilde{\sigma}_{ij}=0$.

Using (24), we find that to zeroth order in the weak fields the sum of the populations is

$$\Pi_1+\Pi_2=(\Lambda_a+\Lambda_b)/\Gamma \tag{27}$$

and the difference is

$$\Pi_1-\Pi_2=\left[\frac{\Lambda_b-\Lambda_a}{\Gamma}\right]\frac{\delta_1}{\bar{\Omega}}\ . \tag{28}$$

In particular, we note that $\Pi_1=\Pi_2$ when $\delta_1=0$, i.e., when the incident light is tuned to resonance.

2. *The density matrix of the dressed atom to second order in the weak fields*

We now describe the influence of the weak fields $\mathbf{E}_2$ and $\mathbf{E}_3$ using a perturbation expansion. The total Hamiltonian is

$$H=H_T+W\ , \tag{29}$$

where H_T is given by (6) and W describes the coupling with the weak fields. At the rotating-wave approximation, W is equal to

$$W=\left[\sum_{m=2,3}\frac{\hbar\Omega_m}{2}e^{-i(\omega_m t+\phi_m)}\right]D_+ + \left[\sum_{m=2,3}\frac{\hbar\Omega_m}{2}e^{+i(\omega_m t+\phi_m)}\right]D_-\ , \tag{30}$$

where ω_2 and ω_3 have been defined in (2b) and (2c) and ϕ_m has a definition similar to ϕ_1,

$$\phi_m=-(\mathbf{k}_m\cdot\mathbf{r}_0+\theta_m),\quad m=2,3\ . \tag{31}$$

As in Sec. II B 1 we calculate $\tilde{\sigma}_{jk}$ instead of σ^p_{jkn}. The equation for $\tilde{\sigma}_{jk}$ is deduced from the master equation,

$$\frac{d}{dt}\tilde{\sigma}_{jk}=\frac{1}{i\hbar}(E_j-E_k)\tilde{\sigma}_{jk}+\left[\frac{d}{dt}\tilde{\sigma}_{jk}\right]_{\rm rel} + \frac{1}{i\hbar}\sum_{m=1,2}(W_{jm}\tilde{\sigma}_{mk}-W_{mk}\tilde{\sigma}_{jm})\ , \tag{32a}$$

where

$$W_{jk}=\frac{\hbar}{2d}\sum_{m=2,3}\Omega_m(d_{jk}e^{i[(\omega_m-\omega_1)t+\phi_m-\phi_1]} + d_{kj}e^{-i[(\omega_m-\omega_1)t+\phi_m-\phi_1]})\ , \tag{32b}$$

d_{kj} being defined as

$$d_{kj}=d\alpha_k\beta_j\ . \tag{33}$$

We now solve Eqs. (32) at second order in weak fields. More precisely, we shall only calculate the matrix elements of $\tilde{\sigma}$ which contribute to the emission of the phase-conjugate wave. The mean value of the electric dipole moment is equal to

$$\bar{D}=\sum_{j,k}(d_{jk}e^{-i(\omega_1 t+\phi_1)}+d_{kj}e^{i(\omega_1 t+\phi_1)})\tilde{\sigma}_{kj}\ . \tag{34}$$

Since the component $\bar{D}_{\rm pc}$ of $\bar{D}$ which radiates the phase-conjugate beam oscillates like $\exp\{-i[(\omega_1+\omega_2-\omega_3)t+\phi_1+\phi_2-\phi_3]\}$, we have only to calculate the components ${}_{\rm pc}\tilde{\sigma}_{kj}$ which oscillate like $\exp\{-i[(\omega_2-\omega_3)t+\phi_2-\phi_3]\}$. The expression of the component $\bar{D}_{\rm pc}$ of the electric dipole moment is thus

$$\bar{D}_{\rm pc}=\sum_{j,k}d_{jk}({}_{\rm pc}\tilde{\sigma}_{kj})e^{-i(\omega_1 t+\phi_1)}+{\rm c.c.} \tag{35}$$

From the zeroth-order solution (26), we find, using the usual perturbative expansion, the first- and second-order solution. Among the second-order terms, we only retain those which can radiate the phase-conjugate beam. We find for the population

$${}_{\rm pc}\tilde{\sigma}_{22}-{}_{\rm pc}\tilde{\sigma}_{11}=-\frac{\Pi_2-\Pi_1}{2d^2}\frac{\Omega_2\Omega_3}{-i(\omega_2-\omega_3)+\Gamma}\Xi \times e^{-i[(\omega_2-\omega_3)t+\phi_2-\phi_3]} \tag{36a}$$

with

$$\Xi = d_{21}^2\left[\frac{1}{-i(\omega_1-\omega_3+\bar{\Omega})+\Gamma}+\frac{1}{i(\omega_1-\omega_2+\bar{\Omega})+\Gamma}\right] + d_{12}^2\left[\frac{1}{-i(\omega_2-\omega_1+\bar{\Omega})+\Gamma}+\frac{1}{i(\omega_3-\omega_1+\bar{\Omega})+\Gamma}\right], \tag{36b}$$

and for the coherence ${}_{pc}\tilde{\sigma}_{12}$,

$${}_{pc}\tilde{\sigma}_{12} = \frac{\Pi_2-\Pi_1}{4d^2}\frac{(d_{22}-d_{11})\Omega_2\Omega_3}{i(\omega_3-\omega_2+\bar{\Omega})+\Gamma}e^{-i[(\omega_2-\omega_3)t+\phi_2-\phi_3]} \times\left[\frac{d_{12}}{i(\omega_3-\omega_1+\bar{\Omega})+\Gamma}+\frac{d_{21}}{i(\omega_1-\omega_2+\bar{\Omega})+\Gamma}\right]. \tag{37}$$

To find ${}_{pc}\tilde{\sigma}_{21}$ we exchange the indices 1 and 2 and we change $\bar{\Omega}$ into $-\bar{\Omega}$.

The four-wave-mixing process will be enhanced when the two denominators in (36) or (37) become resonant. We have presented in Fig. 3 several examples of such processes. Figures 3(a) and 3(b) correspond to a resonance on the population while the other cases [Figs. 3(c)–3(f)] correspond to a resonance on the coherences.

3. *The electric dipole moment in the laboratory frame*

The preceding calculations have been developed in the atomic frame. To find the amplitude of the conjugate wave it is necessary to change the reference frame and to average over the velocity distribution. Using formulas (35)–(37) we obtain the contribution to the electric dipole moment of an atom of velocity **v** located at point **r** at time t. Since (35) is calculated in the atomic frame, we have to calculate $\mathrm{Tr}(DT^{\dagger}\sigma T)$ to find the dipole moment in the laboratory frame. However, this quantity is also equal to $\mathrm{Tr}(TDT^{\dagger}\sigma)=\mathrm{Tr}(D\sigma)$ because T and D act on two different spaces (radiation field and internal atomic variables). Using (2), (5), (8), and (31) we can write $\bar{D}_{pc}(v_z)$ in the laboratory frame as

$$\bar{D}_{pc}(v_z)=\hat{D}_{pc}(v_z)\exp\{-i[(\omega_L+\omega_L'-\omega_L'')t - (\mathbf{k}_1+\mathbf{k}_2-\mathbf{k}_3)\mathbf{r} - \theta_1-\theta_2+\theta_3]\}+\text{c.c.}\,, \tag{38a}$$

where

$$\hat{D}_{pc}(v_z)=\sum_{j,k} d_{jk}({}_{pc}\tilde{\sigma}_{kj})e^{+i[(\omega_2-\omega_3)t+\phi_2-\phi_3]} \tag{38b}$$

is a static term because of the time dependence of (36) and (37). All the atoms located at point **r** radiate a wave of frequency $\omega_L+\omega_L'-\omega_L''$ in the direction $\mathbf{k}_1+\mathbf{k}_2-\mathbf{k}_3$ whatever their velocity is. In the degenerate four-wave mixing case ($\omega_L=\omega_L'=\omega_L''$), the phase-conjugate beam is perfectly phase matched when $\mathbf{k}_1+\mathbf{k}_2=0$. In the case of nondegenerate four-wave mixing, the phase matching is not perfect. However, we shall not discuss this point here because in the nearly degenerate case considered in the experimental part (Sec. III) this problem can be neglected.

To find the amplitude $\hat{\mathscr{D}}_{pc}$ of the dipole created by all the atoms located at point **r** we average (38) over the velocity distribution,

$$\hat{\mathscr{D}}_{pc}=\int \hat{D}_{pc}(v_z)N(v_z)dv_z\,, \tag{39a}$$

where

$$N(v_z)=\frac{N}{u\sqrt{\pi}}\exp\left[-\frac{v_z^2}{u^2}\right], \tag{39b}$$

u being equal to $(2kT/m)^{1/2}$.

We will now establish a symmetry relation concerning $\hat{\mathscr{D}}_{pc}$. In the following we shall consider the case of one or two incident frequencies ω_L and ω_L'. We have thus two frequency detunings in the problem,

$$\delta=\omega_0-\omega_L\,, \tag{40a}$$

$$\delta'=\omega_0-\omega_L'\,. \tag{40b}$$

In the general case $\hat{\mathscr{D}}_{pc}$ is a function of δ and δ'. Using (35)–(37) we easily show that when we change δ, δ', and kv_z into their opposite, $\hat{D}_{pc}(v_z)$ is changed into $-\hat{D}^{*}_{pc}(v_z)$. We then deduce from (38) and (39) that

$$\hat{\mathscr{D}}_{pc}(-\delta,-\delta')=-\hat{\mathscr{D}}^{*}_{pc}(\delta,\delta')\,. \tag{41}$$

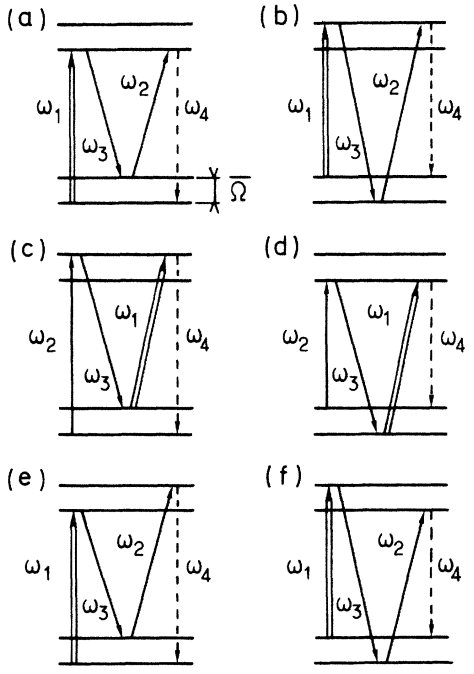

FIG. 3. Resonant four-wave mixing processes in the dressed-atom energy diagram.

4. *Intensity of the phase-conjugate emission*

In the case of a thin optical medium, the amplitude E_{pc} of the phase-conjugate emission can be deduced from the value of $\hat{\mathscr{D}}_{pc}$ (Ref. 5),

$$E_{pc}=\frac{kL}{2i\varepsilon_0}\hat{\mathscr{D}}_{pc}\ , \tag{42}$$

where L is the length of the interaction region. The properties of E_{pc} or $I_{pc}=|E_{pc}|^2$ can thus be directly deduced from the properties of $\hat{\mathscr{D}}_{pc}$ or $|\hat{\mathscr{D}}_{pc}|^2$. In the following we shall only calculate $\hat{\mathscr{D}}_{pc}$, the value of E_{pc} and I_{pc} can then be calculated using (42).

We now use the formalism presented above to predict the line shapes in degenerate and nearly degenerate four-wave mixing.

C. Degenerate four-wave mixing

1. Calculation of the dipole moment

We consider in this section the case where the three beams have the same frequency ω_L. For an atom whose velocity along the z axis is v_z, the three frequencies ω_1, ω_2, and ω_3 in the atomic frame are

$$\omega_1=\omega_L+kv_z\ , \tag{43a}$$

$$\omega_2=\omega_3=\omega_L-kv_z\ . \tag{43b}$$

In this case the examination of formulas (36) and (37) shows that the contribution of the coherences is smaller than the contribution of the populations by a factor of the order of $\Gamma/\bar{\Omega}$. Since $\Gamma\ll\Omega_1$, we can neglect the contribution of the coherences to the electric dipole moment and we obtain for $\hat{D}_{pc}(v_z)$,

$$\hat{D}_{pc}(v_z)=\frac{\Omega_2\Omega_3}{4d^2}\frac{(\Pi_2-\Pi_1)(d_{11}-d_{22})}{\Gamma}\times\left[d_{21}^2\frac{2\Gamma}{(2kv_z+\bar{\Omega})^2+\Gamma^2}+d_{12}^2\frac{2\Gamma}{(2kv_z-\bar{\Omega})^2+\Gamma^2}\right]. \tag{44}$$

We see that there are two resonant denominators in (44). The resonances occur for two velocity groups which are

$$kv_\varepsilon=\frac{-\delta+\varepsilon(3\Omega_1^2+4\delta^2)^{1/2}}{3}\ , \tag{45}$$

where $\varepsilon=\pm1$. To average (44) over the velocity distribution we remark that the resonant denominators vary more rapidly with kv_z than the factors Π_i or d_{ij} which vary on a scale of the order of Ω_1 or $N(v_z)$ which varies on a scale of the order of ku. The assumption (1) enables us to replace the resonant curves of (44) by Dirac δ functions.[9,11] The velocity integration becomes obvious and gives

$$\hat{\mathscr{D}}_{pc}=\frac{\Omega_2\Omega_3}{4d^2}\frac{2\sqrt{\pi}N}{\Gamma ku}\sum_{\varepsilon=\pm1}[(\Pi_2-\Pi_1)(d_{11}-d_{22})d_\varepsilon^2]_{v=v_\varepsilon}\times\left[\frac{2\varepsilon kv_\varepsilon}{(3\Omega_1^2+4\delta^2)^{1/2}}e^{-v_\varepsilon^2/u^2}\right], \tag{46}$$

where $d_+=d_{12}$ and $d_-=d_{21}$. The fact that only two velocity groups contribute to the signal at the secular limit clearly appears on formula (46). These two velocity groups are those for which the four-wave mixing process in the atomic frame is enhanced [Figs. 3(a) and 3(b)] because it corresponds to a nondegenerate four-wave mixing on a Rabi sideband.[9,11]

Using (28) and (33) we make explicit (46) and we find

$$\hat{\mathscr{D}}_{pc}=\frac{d\sqrt{\pi}}{8}\frac{\Omega_2\Omega_3}{\Gamma ku}\frac{N(\Lambda_a-\Lambda_b)}{\Gamma}\frac{\Omega_1}{(3\Omega_1^2+4\delta^2)^{1/2}}\times\sum_{\varepsilon=\pm1}\frac{\varepsilon(\delta-kv_\varepsilon)(3kv_\varepsilon-\delta)^2}{(2kv_\varepsilon)^3}e^{-v_\varepsilon^2/u^2}\ . \tag{47}$$

2. Case of an infinite Doppler width

When $\Omega_1\ll ku$, if we study a range of detunings δ of the order of a few Ω_1, we find that the solution v_ε of (45) is very small compared to u. The factor $e^{-v_\varepsilon^2/u^2}$ can then be replaced by 1. This approximation is similar to the infinite-Doppler-width approximation made in several preceding papers on four-wave mixing.[8,9,11] In this case, we obtain by gathering the two terms of (47)

$$\hat{\mathscr{D}}_{pc}=\frac{d\sqrt{\pi}}{32}\frac{\Omega_2\Omega_3}{\Gamma ku}\frac{N(\Lambda_a-\Lambda_b)}{\Gamma}\frac{\bar{\delta}(15+19\bar{\delta}^2+8\bar{\delta}^4)}{(1+\bar{\delta}^2)^3}\ , \tag{48}$$

where

$$\bar{\delta}=\frac{\delta}{\Omega_1}=\frac{\omega_0-\omega_L}{\Omega_1}\ . \tag{49}$$

The intensity I_{pc} of the phase-conjugate emission versus the frequency detuning is thus a curve whose value is zero for $\delta=0$ and which decreases for large values of δ like $(\Omega_1/\delta)^2$ (Fig. 4). It is interesting to notice that I_{pc} is a function of $\bar{\delta}=\delta/\Omega_1$. When the intensity of the intense-pump beam increases the net effect is only to change the scale on the frequency axis. In particular the maximum value of I_{pc} remains constant even if it occurs for a different value of δ. A similar result has been obtained by Bloch *et al.* for a three-level atom.[8]

It can also be emphasized that even if the curve of Fig. 4 looks like the curves predicted using a motionless atom

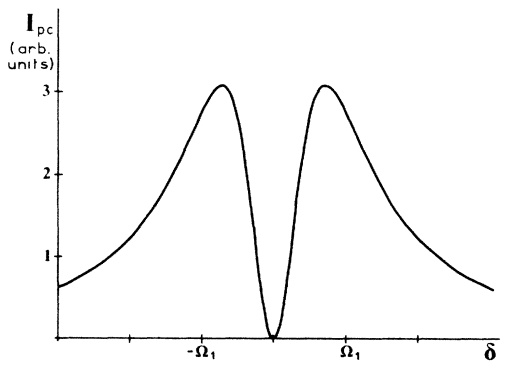

FIG. 4. Intensity of the phase conjugate emission as a function of the frequency detuning δ in the case of backward saturation and assuming an infinite Doppler width (theoretical curve).

theory, its characteristics are considerably different.[11] In particular the maximum value of I_{pc} is much larger for a Doppler-broadened medium.[9,11] [On the other hand, even if (48) differs from the analytical formula obtained in the case of a closed two-level atom,[9] its general characteristics are the same.]

3. Case of a finite Doppler width

When the preceding assumptions ($ku \gg \Omega_1$ and $ku \gg \delta$) are no longer verified, we cannot use the simplified formula (48) and we must use (47). We have represented in Fig. 5 two curves corresponding to the same value of Ω_1, but to two different values of ku. The straight line corresponds to $\Omega_1/ku = \frac{1}{4}$ while the dashed line corresponds to $\Omega_1/ku = 10^{-2}$. The two curves do not differ very much close to the center but they are strongly different in the wings. The effect of Doppler broadening can thus be detected by analyzing the wings of the experimental curves. As we shall see thereafter (Sec. III), this is experimentally an important effect.

As a matter of fact, (47) cannot be used for any values of δ (or Ω_1) since we have neglected at the beginning of the calculation the nonsecular terms. If we consider detunings larger than ku ($\delta > ku$), the ratio secular terms divided by nonsecular terms is of the order of $(\Omega_1^2/\Gamma ku)e^{-v_\varepsilon^2/u^2}$ where v_ε is a solution of (45). A numerical analysis[14] made for different values of Ω_1/ku (Γ/ku being equal to 10^{-2}) shows that (47) is almost exact as long as $\Omega_1/ku \lesssim 1$. Generally speaking (47) can be considered as correct when the solutions v_ε of (45) are such that $|v_\varepsilon| \lesssim u$.

4. Gaussian beam effects

Up to now we have considered the incident beams as plane waves. Experimentally, the preceding theory can only be applied if the transverse dimensions of the probe beam are smaller than the transverse dimension of the pump beams (and if the transit time through the probe beam is longer than Γ^{-1}). Very often, one uses pump and probe beams of similar transverse dimensions. It is thus important to study the line shape in these conditions. Furthermore, it has been shown theoretically[6] that for a motionless atom model, the line shape is strongly different in the case of plane waves and in the case of Gaussian beams. This point has been verified in experiments done in the Rabi limit ($\Omega_1 > ku$) (Ref. 3).

We assume that the pump and probe beams can be described by Gaussian beams. The Rabi frequencies Ω_i ($i = 1,2,3$) are now a function of the position. If the Rayleigh range is much larger than the dimension of the cell, we have

$$\Omega_i(x,y) = \Omega_i^0 \exp[-(x^2+y^2)/2a_i^2] \,. \tag{50}$$

We assume that the transit time through these beams is much longer than Γ^{-1}. When this condition is fulfilled the atom follows adiabatically the intensity variations and the intensity of the phase-conjugate beam is proportional to

$$I_{pc} = X_0^\alpha \int_{X_0}^{+\infty} \frac{dX}{X^\alpha} \frac{(15+19X+8X^2)^2}{(1+X)^6} \tag{51}$$

with

$$X_0 = (\delta/\Omega_1^0)^2 \,, \tag{52a}$$

$$\alpha = a_1^2 \left[\frac{1}{a_2^2} + \frac{1}{a_3^2} \right] . \tag{52b}$$

We have plotted on Fig. 6 two line shapes corresponding to $\alpha = 2$ (three beams of equal diameter) and $\alpha = 5$ (weak beams narrower than the intense-pump beam). In this last case, the line shape is practically identical to the one presented on Fig. 4 for three plane waves because the

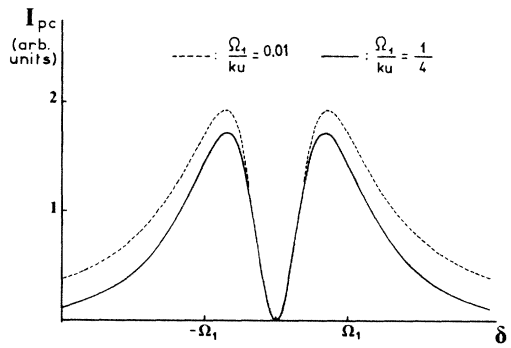

FIG. 5. Influence of the Doppler effect on the phase-conjugate emission in the case of backward saturation. The dashed line which corresponds to $\Omega_1/ku \cong 10^{-2}$ does not differ very much from the curve obtained in the infinite Doppler-width limit. On the other hand, when $\Omega_1/ku = 0.25$, the wings of the curve strongly decrease because of the influence of the Boltzmann factor. (Note that in the experimental situation where ku is constant and Ω_1 varies the scale of the frequency axis varies with Ω_1.)

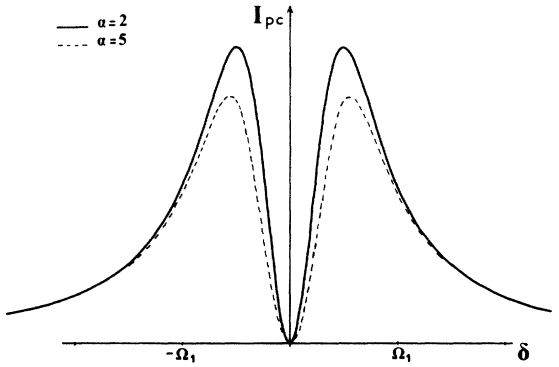

FIG. 6. Effect of the radial distribution of intensity on the phase-conjugate emission. The case $\alpha = 2$ corresponds to three Gaussian beams of same radius, while $\alpha = 5$ corresponds to a situation where the intense-pump-beam radius is much larger than the probe-beam radius. In this last case, the curve is very close to the one obtained with plane waves (Fig. 4). We note that when the three beams have the same radius, the theoretical curve does not qualitatively differ from the curve obtained with plane waves.

conjugate beam is radiated in a volume where the intensity of the intense pump beam is almost constant. The comparison between the cases $\alpha=2$ and 5 shows that the corresponding line shapes do not qualitatively differ. This result is strongly different from the one obtained with motionless atoms.[6] The difference can be easily understood. In the present situation, the contribution of atoms at the edge of the beam is multiplied by $|\Omega_2(r)\Omega_3(r)|^2$ while in the case of motionless atoms this factor is balanced by the fact that the phase-conjugate intensity varies like $\Omega_1^{-4}(r)$.[6] The influence of the edge is thus much more important in the case of motionless atoms.

D. Nearly degenerate four-wave mixing: case of two weak beams of same frequency

The dressed-atom model can also predict the line shape in the case of nearly degenerate four-wave mixing. We consider the case of two light sources of different frequencies ω_L and ω_L'. In the backward-saturation case studied here there are three possible situations according to which beam (intense pump, weak pump, or probe) has a frequency different from the two other beams. We have studied the three cases and we first discuss the case where the intense-pump beam has a frequency ω_L and the two other incident beams a frequency ω_L' [Fig. 7(a)]. The frequency difference between the two light sources is

$$\Delta=\omega_L'-\omega_L \ . \tag{53}$$

The line shape now depends on two parameters: the frequency detuning $\delta=\omega_0-\omega_L$ and Δ.

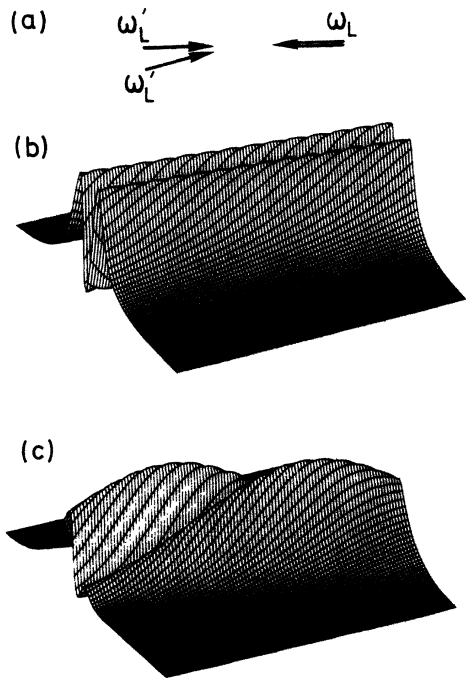

FIG. 7. (a) Four-wave mixing emission in the case of weak beams of same frequency. Variation of I_{pc} vs δ and δ'. The surfaces are calculated (b) in the infinite-Doppler-width limit and (c) in the case $\Omega_1/ku=0.1$.

1. Mean value of the electric dipole moment

In the case considered here [Fig. 7(a)], the two weak beams have the same frequency in the atomic frame,

$$\omega_2=\omega_3=\omega_L'-kv_z \ , \tag{54a}$$

$$\omega_1=\omega_L+kv_z \ . \tag{54b}$$

The situation is thus very similar to the one found in the case of degenerate four-wave mixing. The enhancement of the four-wave mixing process also corresponds to Figs. 3(a) and 3(b), and the results previously obtained can be very easily extended to the present case. For each value of ω_L and ω_L', two velocity groups contribute to the signal at the secular limit. These velocity groups are

$$kv_\varepsilon=\frac{-2\delta'+\delta+\varepsilon[3\Omega_1^2+(\delta+\delta')^2]^{1/2}}{3} \ . \tag{55}$$

As in the degenerate case the velocity integration is performed by replacing the resonant curves by Dirac δ functions and give for the electric dipole moment

$$\hat{\mathscr{D}}_{pc}=\frac{d\sqrt{\pi}}{8}\frac{\Omega_2\Omega_3}{ku}\frac{N(\Lambda_a-\Lambda_b)}{\Gamma}\frac{\Omega_1}{[3\Omega_1^2+(\delta+\delta')^2]^{1/2}} \times\sum_{\varepsilon=\pm1}\varepsilon\frac{\delta_\varepsilon(\delta'+\delta-3\delta_\varepsilon)^2}{(\delta'+\delta-2\delta_\varepsilon)^3}\exp\left[-\frac{(\delta-\delta_\varepsilon)^2}{(ku)^2}\right] \tag{56}$$

with

$$\delta_\varepsilon=\delta-kv_\varepsilon=\frac{2(\delta+\delta')-\varepsilon[3\Omega_1^2+(\delta+\delta')^2]^{1/2}}{3} \ . \tag{57}$$

We see that, apart from the Boltzmann factor, all the other terms only depend on $(\delta+\delta')$.

2. Line shape: case of an infinite Doppler width

When δ, δ', and Ω_1 are much smaller than the Doppler width ku, the Boltzmann factor in (56) can be replaced by 1. In this case, we can gather the contribution of the two velocity groups and obtain a simple analytical formula for $\hat{\mathscr{D}}_{pc}$,

$$\hat{\mathscr{D}}_{pc}=\frac{d\sqrt{\pi}}{4}\frac{\Omega_2\Omega_3}{\Gamma ku}\frac{N(\Lambda_a-\Lambda_b)}{\Gamma} \times\frac{(\bar{\delta}+\bar{\delta}')[60+19(\bar{\delta}+\bar{\delta}')^2+2(\bar{\delta}+\bar{\delta}')^4]}{[4+(\bar{\delta}+\bar{\delta}')^2]^3} \ , \tag{58}$$

where $\bar{\delta}'=\delta'/\Omega_1$. We remark that this formula can be obtained by replacing $\bar{\delta}$ by $(\bar{\delta}+\bar{\delta}')/2$ in the formula (48) obtained in the degenerate case. This corresponds to the fact that in the atomic frame this nearly degenerate four-wave mixing situation is physically equivalent to the one found in the degenerate case.

The surface which represents the variation of the intensity I_{pc} of the phase-conjugate emission versus δ and δ' is shown on Fig. 7(b). In an actual experiment, one of the

frequency detunings (for instance, δ) is kept constant and we vary δ'. The corresponding theoretical curves are associated with a section of the surface $I_{pc}(\delta,\delta')$. These curves have a line shape similar to the one of Fig. 3, but the cancellation of the phase-conjugate emission now occurs when $\delta'=-\delta$.

3. *Line shape: Case of a finite Doppler width*

Using formula (56) it is possible to describe the effect of a finite Doppler width. We have plotted in Fig. 7(c) the intensity of the phase-conjugate emission versus δ and δ' for $\Omega_1/ku=0.1$ (this value has been chosen because it corresponds to a value obtained experimentally). We see that the Boltzmann factor has a strong influence on the shape of the surface. We have shown in Fig. 8 several sections of the surface corresponding to different values of δ. We see that the main effect of the Boltzmann factor on the line shape (I_{pc} versus δ') is to give asymmetrical curves when $\delta\neq 0$.

E. Nearly degenerate four-wave mixing: case of two pump beams of same frequency

We now consider the case where the two pump beams have the same frequency ω_L, the frequency of the probe beam being ω_L' [Fig. 9(a)]. (This situation has been extensively studied in the perturbative limit[5] and for motionless atoms.[10]) We have now a new situation where the three frequencies are different in the atomic frame,

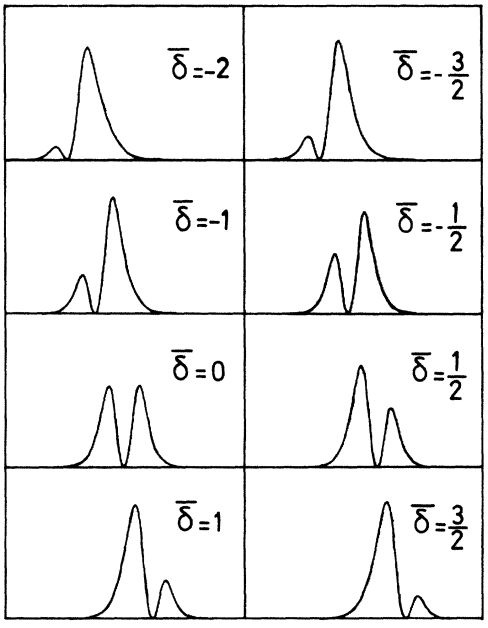

FIG. 8. Four-wave mixing emission with weak beams of same frequency. The theoretical curves describe the variation of I_{pc} obtained for different values of the frequency of the intense pump [$\bar{\delta}=(\omega_0-\omega_L)/\Omega_1$] when the frequency of the weak beam is scanned.

$$\omega_1=\omega_L+kv_z\ , \tag{59a}$$

$$\omega_2=\omega_L-kv_z\ , \tag{59b}$$

$$\omega_3=\omega_L'-kv_z\ . \tag{59c}$$

We now calculate using (36) and (37) for which values of Δ and δ a fully resonant four-wave mixing process can occur in the energy diagram of the dressed atom. The main difference with the preceding case is that we have no longer two velocity groups which fulfill the resonance conditions whatever the values of Δ and δ are. It means that if we keep δ constant and if we vary Δ, we should now observe narrow resonances.

1. *Position of the resonances*

Let us first consider the term corresponding to population (36). In order to have a fully resonant process, we must have $\omega_2=\omega_3$. Using (59b) and (59c) we see that it implies $\omega_L=\omega_L'$, i.e.,

$$\Delta=0\ . \tag{60}$$

This resonance (called Δ_0) is described by the diagram of Figs. 3(a) and 3(b) and corresponds to a degenerate situation.

We now consider the case of resonances occurring on the coherence $\tilde{\sigma}_{12}$ (37). Using (59b) and (59c) we see that a first resonance condition is

$$\Delta=-[\Omega_1^2+(\delta-kv_z)^2]^{1/2}\ , \tag{61}$$

the second resonance condition being either

$$2kv_z=-[\Omega_1^2+(\delta-kv_z)^2]^{1/2} \tag{62}$$

or

$$\Delta-2kv_z=-[\Omega_1^2+(\delta-kv_z)^2]\ . \tag{63}$$

We first consider the resonance Δ_2' obtained using (61) and (62). Using these two equations we find the velocity

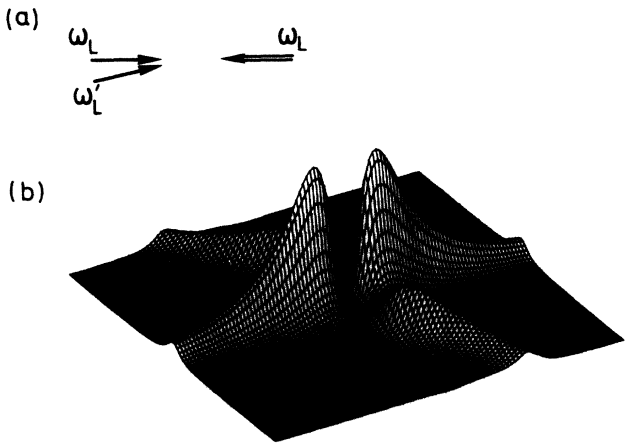

FIG. 9. (a) Four-wave-mixing emission in the case of two pump beams of same frequency. Variation of I_{pc} versus δ and δ'. (b) The surface is obtained in the infinite-Doppler-width limit.

group for which the four-wave mixing is fully resonant and the resonance condition. The velocity group corresponds to the solution v_- of (45) and the resonance condition is

$$\Delta=\Delta_2'=-\tfrac{2}{3}[\delta+(4\delta^2+3\Omega_1^2)^{1/2}]\ . \tag{64}$$

We now consider the resonance Δ_1' associated to (61) and (63). We first observe that this resonance should occur for $v_z=0$ and we then deduce the position of this resonance,

$$\Delta=\Delta_1'=-(\delta^2+\Omega_1^2)^{1/2}\ . \tag{65}$$

If we consider the coherence $\tilde{\sigma}_{21}$ instead of $\tilde{\sigma}_{12}$, we find two new resonances: Δ_1 which is located at

$$\Delta=\Delta_1=(\delta^2+\Omega_1^2)^{1/2} \tag{66}$$

and which also corresponds to the velocity group $v_z=0$, and Δ_2 which is located at

$$\Delta=\Delta_2=\tfrac{2}{3}[-\delta+(4\delta^2+3\Omega_1^2)^{1/2}] \tag{67}$$

and which corresponds to the solution v_+ of (45).

2. Amplitude and width of the resonances: general considerations

The analytical formulas that give $\tilde{\sigma}_{ii}$ and $\tilde{\sigma}_{ij}$ [(36) and (37)] imply that the width of the Δ resonances should be of the order of Γ. To find the shape of the Δ_i resonance we replace in formulas (36) and (37) Δ by $\Delta_i+\xi$, where ξ is a small quantity of the order of Γ and Δ_i is given by (60), (64), (65), (66), or (67). In all these calculations ξ is considered to be small compared to Ω_1 and we shall only retain the terms at lowest order in ξ. Afterwards the mean value of the electric dipole moment is obtained by averaging (38b) over the velocity distribution assuming an infinite Doppler width. The integration over v_z can then be easily performed using the residue theorem.

We do not make such a derivation for the five resonances, since the properties of the Δ_1' and Δ_2' resonances are deduced from the properties of the Δ_1 and Δ_2 resonance using (41).

3. Amplitude and width of the Δ_1 resonance

Using the method that we have presented in Sec. II E 2, we obtain the following value for $\hat{\mathscr{D}}_{pc}$ for values of Δ close to Δ_1 (66):

$$\hat{\mathscr{D}}_{pc}=-\frac{d\sqrt{\pi}}{16}\frac{\Omega_2\Omega_3}{ku}N\frac{\Lambda_a-\Lambda_b}{\Gamma}\frac{\bar{\delta}}{(1+\bar{\delta}^2)}\frac{\Theta(\bar{\delta})}{\Gamma+i(\Delta-\Delta_1)}\ , \tag{68}$$

where $\Theta(\bar{\delta})$ is the Heaviside function which is equal to 0 for $\bar{\delta}<0$ and 1 for $\bar{\delta}>0$. We thus predict that the Δ_1 resonance should only be observed for $\bar{\delta}>0$ at the secular limit. Its width is 2Γ and its intensity is proportional to $\bar{\delta}^2/(1+\bar{\delta}^2)^4$. Let us finally note that the Δ_1 resonance corresponds to the diagram of Fig. 3(f).

4. Amplitude and width of the Δ_1' resonance

Using (41) and (68) we find that the component of the dipole moment which generates the phase-conjugate beam close to the Δ_1' resonance (65) is

$$\hat{\mathscr{D}}_{pc}=-\frac{d\sqrt{\pi}}{16}\frac{\Omega_2\Omega_3}{ku}N\frac{\Lambda_a-\Lambda_b}{\Gamma}\frac{\bar{\delta}}{(1+\bar{\delta}^2)^2}\frac{\Theta(-\bar{\delta})}{\Gamma+i(\Delta-\Delta_1')}\ . \tag{69}$$

The Δ_1' resonance can only be observed for $\bar{\delta}<0$ (at the secular limit). Its width is also equal to 2Γ. This resonance corresponds to the diagram of Fig. 3(e).

5. Amplitude and width of the Δ_2 resonance

For Δ close to Δ_2 the mean value of the dipole moment $\hat{\mathscr{D}}_{pc}$ is

$$\hat{\mathscr{D}}_{pc}=\frac{d\sqrt{\pi}}{16}\frac{\Omega_2\Omega_3}{ku}\frac{\Lambda_a-\Lambda_b}{\Gamma}\times\frac{(\bar{\Delta}_2-2\bar{\delta})(\frac{3}{2}\bar{\Delta}_2-\bar{\delta})^2\Theta(\frac{1}{2}-\bar{\delta})}{\bar{\Delta}_2^3(3+4\bar{\delta}^2)^{1/2}\left[i(\Delta-\Delta_2)+\dfrac{2\Gamma\bar{\Delta}_2}{(3+4\bar{\delta}^2)^{1/2}}\right]}\ , \tag{70}$$

where $\bar{\Delta}_2=\Delta_2/\Omega_1$ and Δ_2 is given in (67). At the secular limit this resonance should only be observed for $\delta<\Omega_1/2$. The width is equal to

$$\gamma_2=\frac{4\Gamma\bar{\Delta}_2}{(3+4\bar{\delta}^2)^{1/2}} \tag{71}$$

and its asymptotic value for $\delta\ll-\Omega_1$ is 4Γ. This resonance corresponds to the diagram of Fig. 3(d).

6. Amplitude and width of the Δ_2' resonance

The properties of this resonance are found using (41) and (70). Around the Δ_2' resonance (64), $\hat{\mathscr{D}}_{pc}$ is equal to

$$\hat{\mathscr{D}}_{pc}=\frac{d\sqrt{\pi}}{16}\frac{\Omega_2\Omega_3}{ku}N\frac{\Lambda_a-\Lambda_b}{\Gamma}\times\frac{(\bar{\Delta}_2'-2\bar{\delta})(\frac{3}{2}\bar{\Delta}_2'-\bar{\delta})^2\Theta(\frac{1}{2}+\bar{\delta})}{\bar{\Delta}_2'^3(3+4\bar{\delta}^2)^{1/2}\left[i(\Delta-\Delta_2')+\dfrac{2\Gamma\bar{\Delta}_2'}{(3+4\bar{\delta}^2)^{1/2}}\right]}\ , \tag{72}$$

where $\bar{\Delta}_2'=\Delta_2'/\Omega_1$. This resonance corresponds to the diagram of Fig. 3(c).

7. Amplitude and width of the Δ_0 resonance

Using the same method we find the value of $\hat{\mathscr{D}}_{pc}$ around the Δ_0 resonance (60),

$$\hat{\mathscr{D}}_{pc}=\frac{d\sqrt{\pi}}{32}\frac{\Omega_2\Omega_3}{ku}N\frac{\Lambda_a-\Lambda_b}{\Gamma}\times\frac{\bar{\delta}(15+19\bar{\delta}^2+8\bar{\delta}^4)}{(1+\bar{\delta}^2)^3}\frac{1}{i\Delta+\Gamma}\ . \tag{73}$$

When Δ varies, we obtain a resonance when $\Delta=0$. The width of the resonance is 2Γ and its intensity is equal to the value (48) predicted for the degenerate case.

8. Conclusion

Using the preceding formulas we have calculated the surface which represents the variation of the phase-conjugate intensity versus δ and δ' [Fig. 9(b)]. For a given value of δ, when we vary Δ we generally observe only two resonances. In fact, the Δ_1 and Δ_1' resonances are about 2 orders of magnitude smaller than the Δ_0, Δ_2, and Δ_2' resonances and are not visible on the same scale. The main resonances are Δ_0 and Δ_2 for $\delta<0$ and Δ_0 and Δ_2' for $\delta>0$. It can be emphasized that the resonances which are important in the geometry of Fig. 9(a) do not correspond to $v_z=0$. For each value of δ, the velocity group changes and the relation between the position of the resonances and the dynamic Stark effect is not obvious.

F. Nearly degenerate four-wave mixing: The intense pump beam and the probe beam have the same frequency

We finally consider the case where the intense-pump beam and the probe beam have the same frequency ω_L, the frequency of the weak pump beam being ω_L' [Fig. 10(a)]. In the atomic frame, the frequencies now become

$$\omega_1=\omega_L+kv_z\ , \tag{74a}$$

$$\omega_2=\omega_L'-kv_z\ , \tag{74b}$$

$$\omega_3=\omega_L-kv_z\ . \tag{74c}$$

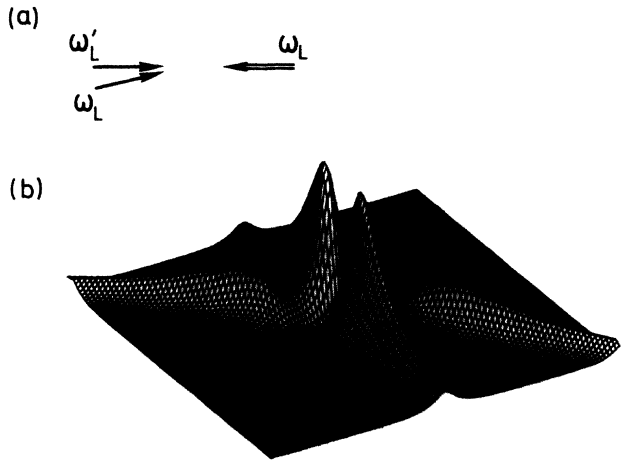

FIG. 10. (a) Four-wave mixing emission in the case when the frequency ω_L of the weak pump beam is different from the frequency ω_L of the intense pump and of the probe. Variation of I_{pc} vs δ and δ'. (b) The surface is obtained in the infinite-Doppler-width limit.

The analysis of formulas (36) and (37) shows that the resonances occur for the values of Δ found in Sec. II E but that their intensities are now completely different.

1. Amplitude and width of the Δ_1 resonance

Using the method presented in Sec. II E 2 we calculate $\hat{\mathscr{D}}_{pc}$ for Δ close to Δ_1, Δ_1 being given in (66),

$$\hat{\mathscr{D}}_{pc}=-\frac{d\sqrt{\pi}}{16}\frac{\Omega_2\Omega_3}{ku}N\frac{\Lambda_a-\Lambda_b}{\Gamma}\times\frac{\bar{\delta}[\bar{\delta}+(1+\bar{\delta}^2)^{1/2}]^2}{(1+\bar{\delta}^2)^2}\frac{\Theta(\bar{\delta})}{\Gamma-i(\Delta-\Delta_1)}\ . \tag{75}$$

We see that the Δ_1 resonance can only be observed for $\delta>0$ and that its width is 2Γ. This resonance is described by the diagram of Fig. 3(c).

2. Amplitude and width of the Δ_1' resonance

Using (41) and (75) we find for Δ close to Δ_1' (65),

$$\hat{\mathscr{D}}_{pc}=-\frac{d\sqrt{\pi}}{16}\frac{\Omega_2\Omega_3}{ku}N\frac{\Lambda_a-\Lambda_b}{\Gamma}\frac{\bar{\delta}[(1+\bar{\delta}^2)^{1/2}-\bar{\delta}]^2}{(1+\bar{\delta}^2)^2}\times\frac{\Theta(-\bar{\delta})}{\Gamma-i(\Delta-\Delta_1')}\ . \tag{76}$$

The Δ_1' resonance can only be observed for $\delta<0$ and its width is 2Γ. This resonance is described by the diagram of Fig. 3(d).

3. Amplitude and width of the Δ_2 resonance

For Δ close to Δ_2 (67), we find

$$\hat{\mathscr{D}}_{pc}=\frac{d\sqrt{\pi}}{16}\frac{\Omega_2\Omega_3}{ku}N\frac{\Lambda_a-\Lambda_b}{\Gamma}\times\frac{(\bar{\Delta}_2-2\bar{\delta})\times[\Theta(\frac{1}{2}-\bar{\delta})]}{\bar{\Delta}_2^3(3+4\bar{\delta}^2)^{1/2}\left[\dfrac{2\Gamma\Delta_2}{(3\Omega_1^2+4\delta^2)^{1/2}}-i(\Delta-\Delta_2)\right]}\ . \tag{77}$$

The Δ_2 resonance should only be observed when $\delta<\Omega_1/2$. The width of the resonance is given by (71). The diagram of Fig. 3(e) corresponds to this situation.

4. Amplitude and width of the Δ_2' resonance

Using (41) and (77) we find for Δ close to Δ_2' (64),

$$\hat{\mathscr{D}}_{pc}=\frac{d\sqrt{\pi}}{16}\frac{\Omega_2\Omega_3}{ku}N\frac{\Lambda_a-\Lambda_b}{\Gamma}\times\frac{(\bar{\Delta}_2'-2\bar{\delta})\times[\Theta(\frac{1}{2}+\bar{\delta})]}{\bar{\Delta}_2'^3(3+4\bar{\delta}^2)^{1/2}\left[\dfrac{2\Gamma\Delta_2'}{(3\Omega_1^2+4\delta^2)^{1/2}}-i(\Delta-\Delta_2')\right]}\ . \tag{78}$$

The diagram of Fig. 3(f) corresponds to this resonance.

5. Amplitude and width of the Δ_0 resonance

The value of $\hat{\mathscr{D}}_{pc}$ for this resonance is identical to the value (73) found in Sec. II E 7. Here also, this resonance corresponds to the diagrams of Figs. 3(a) and 3(b).

6. Conclusion

Using the preceding formulas, we have plotted in Fig. 10(b) the intensity of the phase-conjugate emission versus δ and δ'. As in Sec. II E, when we vary Δ we observe two resonances. However, these resonances are now Δ_0, Δ_1, and Δ_1', the Δ_2 and Δ_2' resonances having an intensity weaker by 2 orders of magnitude. This point is clearly very interesting because the Δ_1 and Δ_1' resonance corresponds to the velocity group $v_z=0$. The geometry of Fig. 10(a) enables us to directly measure in an atomic vapor the dynamic Stark effect without any correction for the Doppler effect. Another advantage of the geometry of Fig. 10(a) is that the Δ_1 and Δ_1' resonances are expected to be narrower than the Δ_2 and Δ_2' resonances. We thus expect that the spectra obtained in the geometry of Fig. 10(a) should contain narrower resonances than the spectra obtained in the geometry of Fig. 9(a).

In conclusion, the comparison between the results obtained in Secs. II E and II F shows that the best conditions to observe the dynamic Stark effect in an atomic vapor by nearly degenerate four-wave mixing are those of Sec. II F. This explains some of the problem encountered by Steel and Lind[15] in observing the dynamic Stark effect in sodium vapor using two pump beams of the same frequency. (In fact, their experiment was done with two beams of the same intensity. In that situation, the Rabi frequency is spatially modulated in the laboratory frame and the theory is more complex than the one derived in Sec. II E.)

III. EXPERIMENTAL STUDY

A. Description of the experimental setup

1. The neon cell

We have performed the experiments in a neon discharge. Even if the four-wave mixing in neon is less efficient than in sodium, the simplicity of the neon spectrum, and in particular the lack of hyperfine structure in ^{20}Ne, makes this element more interesting for quantitative comparisons. We recall in Fig. 11 some of the excited levels of neon. Most of our experiments have been done on the 607-nm transition which couples the $1s_4$ ($J=1$) resonance level of neon and the $^2p_3$ ($J=0$) excited level. The main interest of this transition is that it corresponds to a perfect two-level atom when the incident beams have the same polarization and a perfect three-level atom when cross-polarized pumps are used.[7,16] Some experiments have also been performed on the 640-nm transition which couples the $1s_5$ ($J=2$) metastable level and the $2p_9$ ($J=3$) excited level. The four-wave mixing process is more efficient (by about 1 order of magnitude) on this transition but the difference of the Clebsch-Gordan coefficients and the Zeeman optical pumping makes a quantitative interpretation more problematic. The maximum

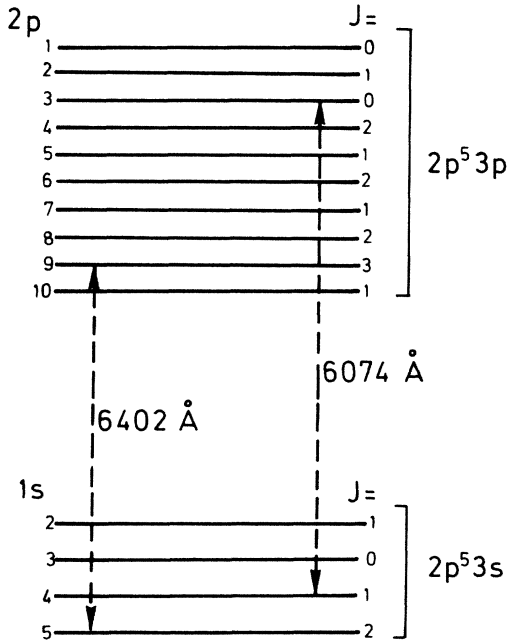

FIG. 11. Energy levels of neon. Our experiments are done on the $1s_5$-$2p_9$ transition (6402 Å) and on the $1s_4$-$2p_3$ transition (6074 Å).

value of I_{pc}/I_3 (phase-conjugate reflectivity) on the 640-nm transition is 0.5×10^{-2}. This value is coherent with the assumption of a thin optical medium. We have used a 5-cm quartz cell, filled with 0.6 Torr of neon in the case of the 607-nm transition and with 0.1 Torr in the case of the 640-nm transition.

2. The light source

The experiments have been done with a homemade cw dye laser[17] pumped by an Ar^+ laser. This single-mode dye laser delivers about 0.5 W at 607 nm using Rhodamine 590 and 0.4 W at 640 nm using a mixture of Rhodamine 590 and 640.

3. The four-wave mixing process

In the degenerate four-wave mixing experiment, the three beams come from the same laser. Using a thick glass plate L_1 (see Fig. 12), we separate two weak beams

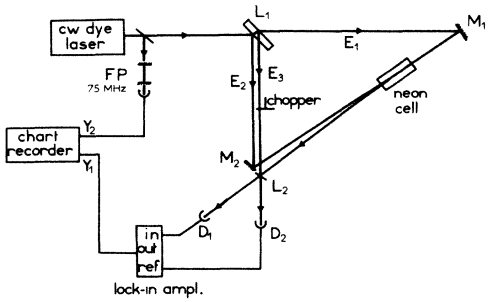

FIG. 12. Experimental setup.

E_2 and E_3 from the intense beam E_1. The intensities of I_2 and I_3 are less than $10^{-2}I_1$. The mirrors M_1 and M_2 are used to have a perfect superposition of the pump beams inside the experimental cell. The probe beam E_3 is reflected in the cell by a semitransparent mirror L_2. The angle between E_2 and E_3 is of the order of 10^{-2} rad.

In the case of nearly degenerate four-wave mixing we used two identical light sources. The laser whose frequency is scanned is controlled using a 75-MHz free-spectral-range Fabry-Perot (FP) interferometer. We use another Fabry-Perot interferometer (1.5-GHz free spectral range) to determine when the two frequencies ω_L and ω_L' are equal.

4. Detection

Before being transmitted into the neon cell using L_2, the probe-beam intensity is modulated at 800 Hz. The intensity of the phase-conjugate beam is detected with the photomultiplier D_1 and analyzed with a lock-in amplifier. We record on the Y_1 trace of a chart recorder the intensity of the phase-conjugate emission and on the Y_2 trace the transmission peaks of a 75-MHz free-spectral-range interferometer.

5. The relative values of Γ, Ω_1, and ku

Since our theoretical model has been developed for a peculiar hierarchy of the parameters Γ, Ω_1, and ku, it is important to check that (1) is fulfilled in our experimental situation. The Doppler width ku at 300 K in neon is of the order of 0.8 GHz. To estimate the value of the relaxation rate Γ, we have measured the width of a saturated absorption line shape. We have found 20 MHz for the half width at half maximum in the case of the 607-nm line and 15 MHz in the case of the 640-nm line. (These values include the jitter of the laser.) With an incident power equal to $P_1=10$ W/cm^2 we obtain $\Omega_1\simeq 100$ MHz for the 607-nm line. In the case of the 640-nm line we have several Clebsch-Gordan coefficients and we can only define a mean value of Ω_1 which is of the order of 160 MHz.

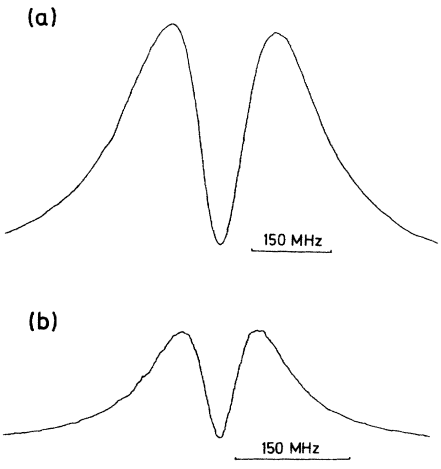

FIG. 13. Degenerate four-wave mixing on the 6402-Å transition in neon. (a) Experimental recording of I_{pc} obtained with a probe-beam radius smaller than the pump-beam radius (case where the plane wave theory can be applied). (b) Recording in a situation where the three incident beams have the same radius.

B. Experimental study of degenerate four-wave mixing

1. Case of the 640-nm line

a. Variation with the pump beam intensity. We show in Fig. 13(a) a curve obtained with three linearly polarized beams of incident intensity equal to $P_1\simeq 10$ W/cm^2, $P_2\simeq 0.05$ W/cm^2, and $P_3\simeq 0.01$ W/cm^2. The probe beam has been focussed at the center of the pump beams to be in a situation where a plane wave theory can be applied. The general features of this curve qualitatively correspond to theory (see Fig. 4). We have measured the distance between the two maxima of Fig. 13(a) for different values of P_1 and plotted this distance as a function of P_1 in logarithmic scale in Fig. 14. We see that the points are on a straight line of slope $\frac{1}{2}$, in agreement with theory.

b. Gaussian beam effects. If we do not focus the probe beam the three incident beams have the same radius. The phase-conjugate intensity versus δ, obtained in these conditions, is shown in Fig. 13(b). This line shape is in qualitative agreement with the theoretical curve of Fig. 6. In particular, contrary to the case $\Omega_1 > ku$ experimentally studied by Kleinmann *et al.*[3] the line shapes of Fig. 13(a) and Fig. 13(b) are very similar.

c. Discussion. We have not tried to perform a qualitative comparison because the 640-nm line is not an excellent situation to test the model of Fig. 1(b). The lower

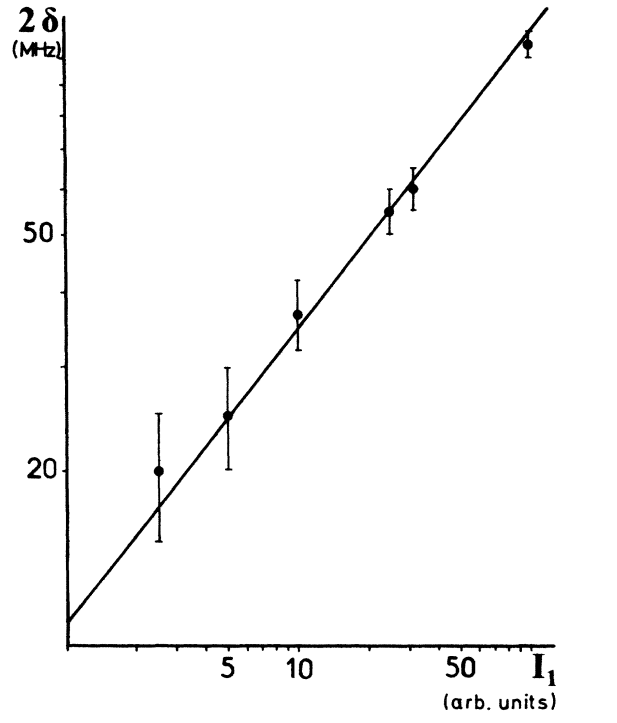

FIG. 14. Distance between the two maxima of emission in degenerate four-wave mixing as a function of the intensity of the pump beam. We find a square-root law in agreement with theory.

$J=2$ level is a metastable level and the situation should be quantitatively discussed using the theory developed for a resonance line.[9,11] Furthermore, because of the different Zeeman sublevels, it is not possible to consider that we have a real two-level atom. It is the reason why most of our quantitative experiments have been developed on the 607-nm line.

2. *Case of the 607-nm line*

We show in Fig. 15(a) a line shape obtained at 607-nm for $P_1=20$ W/cm^2 ($\Omega_1=165$ MHz). This curve has been obtained with a probe beam focussed at the center of the pump beams. We have compared this curve with theoretical points obtained using formula (48) valid for an infinite Doppler width. The agreement is rather good at the center of the line but a large discrepancy is observed on the wings. If instead of (48) we used (47) and take into account the finite Doppler width effect we obtain the points of Fig. 15(b) which are in excellent agreement with the experimental results. This study clearly shows that a quantitative agreement can be obtained when the Doppler velocity distribution is included in the theory.

C. Experimental study of nearly degenerate four-wave mixing

We describe here experiments done on the 607-nm line of neon with three incident beams which have the same linear polarization. The light at frequency ω_L and ω'_L come from two different lasers. The frequency ω_L of the intense beam is kept constant and we record the intensity of the four-wave mixing emission versus ω'_L. This experiment is repeated for several values of $\delta=\omega_0-\omega_L$.

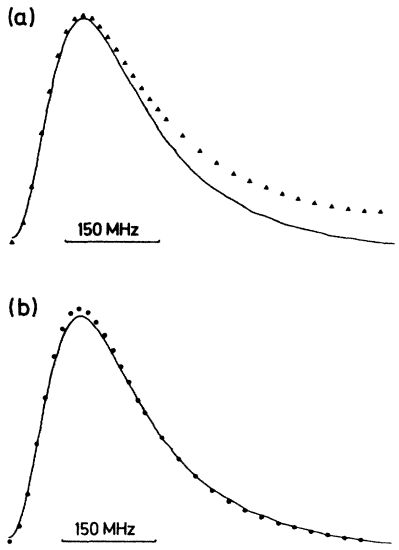

FIG. 15. Quantitative comparison between experiment and theory in the case of degenerate four-wave mixing at 6074 Å. The experimental curve obtained for I_{pc} vs δ ($\delta\geq 0$) is compared with theoretical points calculated using (a) an infinite Doppler width and (b) a realistic Doppler width. The excellent agreement obtained in this last case demonstrates the influence of the Boltzmann factor.

1. *Case of two weak beams of the same frequency*

We show in Fig. 16 several recordings of the four-wave mixing emission obtained for several values of $\delta=\omega_0-\omega_L$. The value of the Rabi frequency of the intense-pump beam Ω_1 is 100 MHz. The asymmetry observed for $\delta\neq 0$ is related to the influence of the Boltzmann factor. Indeed, the comparison with the theoretical curves of Fig. 8 is very good and shows that a quantitative comparison needs to take into account the Maxwell-Boltzmann velocity distribution.

2. *Case of a probe beam and an intense pump beam of the same frequency*

We now present the situation theoretically studied in Sec. II F. The case of two pump beams of equal frequency will be discussed afterwards and compared to the results of this section.

a. Position of the resonances. The experiments are done by scanning the frequency ω'_L of the weak pump wave. We have done several recordings for -300 MHz $\leq\delta\leq 600$ MHz. We show in Fig. 17 an experimental curve recorded for $\delta=250$ MHz. We observe two resonances which are Δ_0 and Δ_1. The positions of the resonances are reported in Fig. 18 where they are compared to

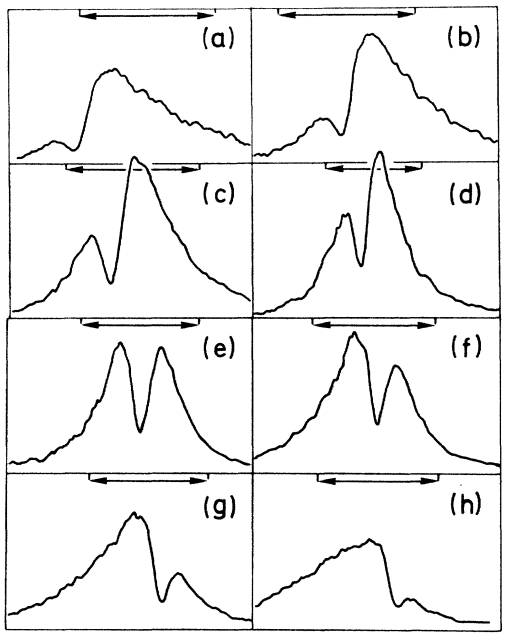

FIG. 16. Nearly degenerate four-wave mixing at 6074 Å. Case of two weak beams of the same frequency. The different experimental recordings of I_{pc} correspond to different values of $\delta=\omega_0-\omega_L$. They are obtained by scanning the frequency ω'_L of the weak pump beam. For each value the distance between the two arrows corresponds to a scanning of 0.75 GHz. The value of Ω_1 is 90 MHz. The different curves correspond to $\delta=-0.6$ GHz (a), -0.45 GHz (b), -0.3 GHz (c), -0.15 GHz (d), 0 (e), 0.15 GHz (f), 0.3 GHz (g), and 0.45 GHz (h). The asymmetry observed when $\delta\neq 0$ is related to Boltzmann factors which differ for $\delta'>-\delta$ and $\delta'<-\delta$ (see theoretical curves, Fig. 8).

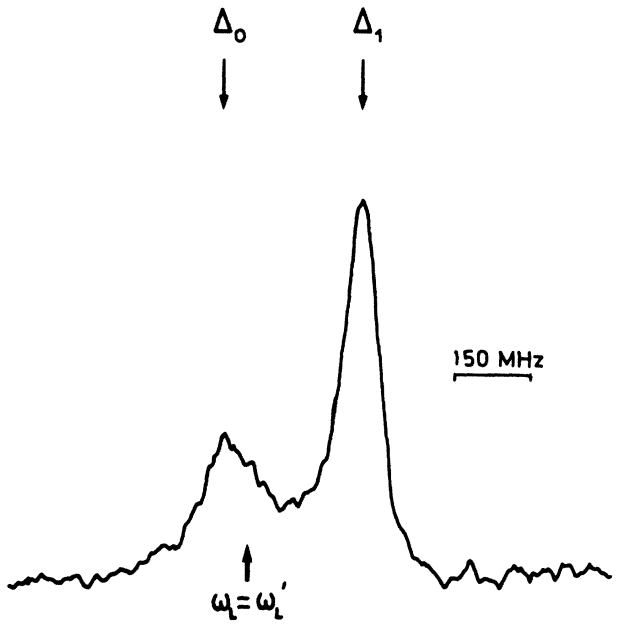

FIG. 17. Nearly degenerate four-wave mixing at 6074 Å. Experimental recording of the four-wave mixing emission. The intense pump beam and the probe have the same frequency ω_L ($\omega_0-\omega_L=250$ MHz). The frequency of the weak pump beam is scanned. Two resonances (Δ_0 and Δ_1) are observed.

the theoretical values (obtained with $\Omega_1=90$ MHz). We note that the Δ_1 and Δ_1' resonances correspond to the velocity group $v_z=0$ and that they are directly connected with the energy levels of the dressed atom. The width ($\sim$75 MHz) of the Δ_1 and Δ_1' resonance is much smaller than the Doppler width. We have thus observed a Doppler-free spectrum of atoms dressed by optical photons in a cell.[18]

We have observed neither the Δ_2 nor the Δ_2' resonance. This is in good agreement with the theoretical predictions

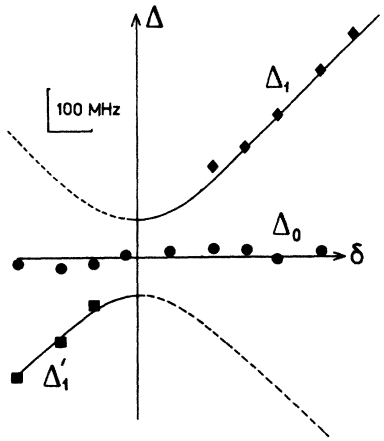

FIG. 18. Nearly degenerate four-wave mixing at 6074 Å. Position of the resonances vs frequency of the intense pump beam (which is equal to the frequency of the probe beam). The experimental points are compared with a theoretical curve obtained in Sec. II F.

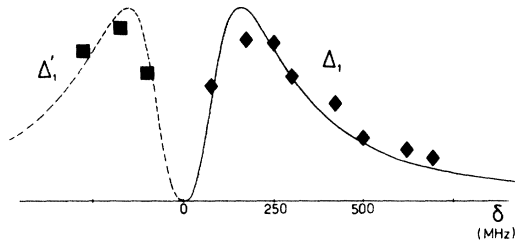

FIG. 19. Nearly degenerate four-wave mixing at 6074 Å. Intensity of the Δ_1 and Δ_1' resonances vs frequency of the intense pump beam. The experimental points are compared with the theoretical curves obtained in Sec. II F.

(Sec. II F 6) since we have calculated that the intensity of Δ_2 and Δ_2' should be 100 times smaller than the intensity of Δ_1 and Δ_1'.

b. Widths of the resonance. The width of the Δ_1 resonance of Fig. 17 is 75 MHz. This curve is broader than the saturated absorption line whose width is 40 MHz. Theoretically we have predicted that the two curves should have the same width. The difference comes from the fact that we use two independent light sources. We must also take into account the residual Doppler effect induced by the angle between $\mathbf{E}_2$ and $\mathbf{E}_3$.

When δ varies, the width of the Δ_1 resonance remains almost constant and of the order of 70 MHz. This behavior is in agreement with our theoretical calculations which predict that the width of Δ_1 should remain constant (see Sec. II F 1).

c. Intensity of the resonances. We have plotted in Fig. 19 the experimental intensities of the Δ_1 and Δ_1' resonances versus δ. These points are compared with the theoretical curve calculated in Sec. II F. We see that the agreement is good. However, we must add that the relative intensities of Δ_1 and Δ_0 differ from the theoretical prediction. For large values of δ we find a ratio equal to 3 while the theory predicts a ratio equal to 1. We have shown[19] that this discrepancy comes from the fact that we have used one single relaxation time Γ to describe the relaxation of all the quantities: optical coherence, population of levels $|a\rangle$ and $|b\rangle$, etc. If we used a more realis-

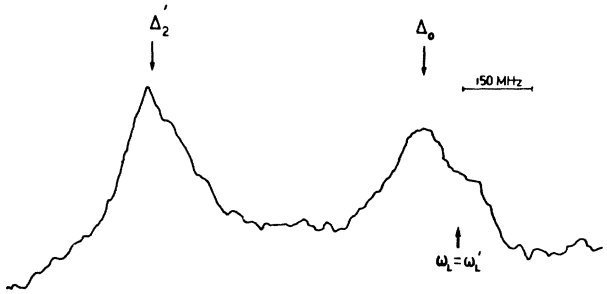

FIG. 20. Nearly degenerate four-wave mixing at 6074 Å. Case of two pump beams of the same frequency. Intensity of the phase-conjugation emission vs the frequency of the probe beam. The pump frequency detuning is 400 MHz. The two observed resonances are Δ_0 and Δ_2'.

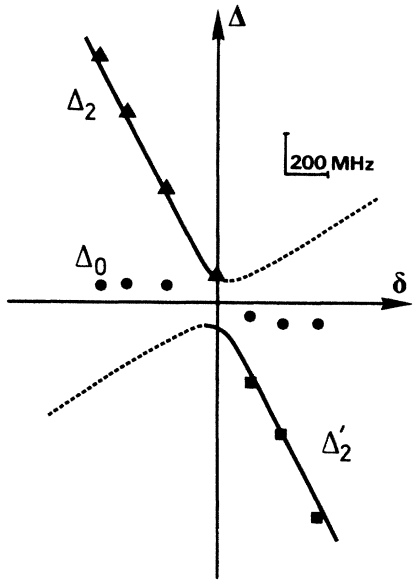

FIG. 21. Nearly degenerate four-wave mixing at 6074 Å. Case of two pumps of the same frequency. Position of the resonances vs frequency of the pump. The experimental points are compared with the theoretical curve obtained in Sec. II E.

tic model with different relaxation rates, we can explain this difference.

3. *Case of two pump beams of the same frequency*

a. Position of the resonances. The experimental curves are obtained by scanning the frequency ω'_L of the probe beam. We have done several recordings for -500 MHz $\leq\delta\leq 500$ MHz. A recording obtained for $\delta=400$ MHz is shown in Fig. 20. We observe two resonances which can be identified as Δ_0 and Δ'_2. We have plotted the experimental position of the resonances (Fig. 21) together with the theoretical prediction for the Δ_0, Δ_2, and Δ'_2 resonances (Ω_1 is equal to 90 MHz). We can note that the Δ_1 and Δ'_1 resonances have not been observed in agreement with the theoretical predictions of Sec. II E 8.

b. Width and intensity of the resonances. The width of the Δ'_2 resonance of Fig. 20 is of the order of 150 MHz. We recall that the theory predicts a width equal to 4Γ when $|\delta|\gg\Omega_1$. This width is larger than the width of the Δ_1 resonance of Fig. 17. This is in agreement with our theoretical model which predicts that the ratio should be equal to 2.

Concerning the intensities, we observe only the Δ_0, Δ_2, and Δ'_2 resonances. This is in agreement with our theoretical model which predicts that Δ_1 and Δ'_1 should be 2 orders of magnitude smaller. The experimental variation of the intensities of Δ_2 and Δ'_2 versus δ is also in agreement with theory. On the other hand, we find, as in Sec. III C 2 that the relative intensities of Δ_0 and Δ_2 differ by a factor of 3 from the theoretical prediction. Here also, a more realistic model for the relaxation (as in Sec. III C 2 c) permits an understanding of this point.

IV. CONCLUSION

In conclusion, we have developed a new theoretical approach which makes use of the dressed-atom model, to study the effect of saturation in four-wave mixing. We have done experiments in neon to verify the validity of the model. Our main results follow.

We have verified that this theory permits us to correctly interpret most of our experimental observation both in degenerate and nondegenerate four-wave mixing.

As in the preceding study of Bloch and Ducloy,[8] our experimental results cannot be interpreted using a motionless-atom model. On the other hand, we have shown that a quantitative analysis of the experimental observation cannot be done with the assumption of an infinite Doppler width. A quantitative understanding needs to take into account the correct Boltzmann factor of the velocity distribution.

In the case of nearly degenerate four-wave mixing, we have shown that the phase-conjugate emission is strongly different according to the choice of the beam which has a different frequency. We have also shown that narrow resonances can be observed which correspond to a Doppler-free spectrum of atoms dressed by optical photons.

We have considered in this paper the case of three incident beams of same polarization. Another important situation corresponds to the case of cross-polarized beams. We will show in a forthcoming paper[20] that the dressed-atom model also permits us to clarify the underlying physics in that situation and leads to predictions which are in agreement with the experimental results.

The study presented here has the great advantage in clarifying the real effect of Doppler broadening in nearly degenerate four-wave mixing. However, the results cannot be directly applied to experiments in optical phase conjugation where the two pump beams generally have similar intensity. In the case of two-level atoms, a theoretical study of the effect of two saturating pump beams is not a straightforward extension of the present model. If the case $\Gamma<\Omega_2\ll\Omega_1$ can be included in the theory,[11] the case $\Omega_1\sim\Omega_2\gg\Gamma$ needs a special and more complicated analysis, this last situation being similar to the problem of a spin $\frac{1}{2}$ interacting with a static field and two intense nearly resonant radio-frequency fields. On the other hand, in the case of three-level atoms, the effect of two intense cross-polarized pump beams can be solved analytically. Thus, we feel that a closest approach to situations usually encountered in optical phase conjugation should be easier in the case of cross-polarized pump beams.

ACKNOWLEDGMENTS

The Laboratoire de Spectroscopie Hertzienne de l'Ecole Normale Supérieure is "associé au Centre National de la Recherche Scientifique."

[1]*Optical Phase Conjugation,* edited by R. Fisher (Academic, New York, 1983).

[2]R. W. Hellwarth, J. Opt. Soc. Am. **67**, 1 (1977), A. Yariv and D. M. Pepper, Opt. Lett. **1**, 16 (1977).

[3]D. H. Bloom, P. F. Liao and N. P. Economou, Opt. Lett. **2**, 58 (1978); R. C. Lind and D. G. Steel, *ibid.* **6**, 554 (1981); B. Kleinmann, F. Trehin, M. Pinard, and G. Grynberg, J. Opt. Soc. Am. B **2**, 704 (1985); P. Kumar, Opt. Lett. **10**, 74 (1985).

[4]E. Le Bihan, P. Verkerk, M. Pinard, and G. Grynberg, Opt. Commun. **56**, 202 (1985); E. Le Bihan, M. Pinard, and G. Grynberg, Opt. Lett. **11**, 159 (1986); M. Pinard, D. Granclément, and G. Grynberg, Europhys. Lett. (to be published); J. R. R. Leite, P. Simoneau, D. Bloch, S. Leboiteux, and M. Ducloy, *ibid.* (to be published).

[5]S. M. Wandzura, Opt. Lett. **4**, 208 (1979); J. Nielsen and A. Yariv, J. Opt. Soc. Am. **71**, 180 (1981); M. Ducloy and D. Bloch, J. Phys. (Paris) **42**, 711 (1981); **43**, 57 (1982).

[6]R. L. Abrams and R. C. Lind, Opt. Lett. **2**, 94 (1978); **3**, 205 (1978); G. J. Dunning and D. G. Steel, IEEE J. Quantum Electron. **QE-18**, 3 (1982); G. P. Agrawal, A. Van Lerberghe, P. Aubourg, and J. L. Boulnois, Opt. Lett. **7**, 540 (1982); G. Grynberg, B. Kleinmann, and M. Pinard, Opt. Commun. **47**, 291 (1983); S. Stuut and M. Sargent III, J. Opt. Soc. Am. B **1**, 95 (1984); M. Pinard, B. Kleinmann, and G. Grynberg, Opt. Commun. **51**, 281 (1984).

[7]D. Bloch, R. K. Raj, K. S. Peng, and M. Ducloy, Phys. Rev. Lett. **49**, 719 (1982).

[8]D. Bloch and M. Ducloy, J. Opt. Soc. Am. **73**, 635 (1983); **73**, 1844 (1983).

[9]G. Grynberg, M. Pinard, and P. Verkerk, Opt. Commun. **50**, 261 (1984).

[10]D. J. Harter and R. W. Boyd, IEEE J. Quantum Electron. **QE-16**, 1126 (1980); D. J. Harter and R. W. Boyd, Phys. Rev. A **29**, 739 (1984).

[11]G. Grynberg, M. Pinard, and P. Verkerk, J. Phys. (Paris) **47**, 617 (1986).

[12]M. Ducloy and D. Bloch, Opt. Commun. **47**, 351 (1983).

[13]C. Cohen-Tannoudji, in *Frontiers in Laser Spectroscopy,* edited by R. Balian, S. Haroche, and S. Liberman (North Holland, Amsterdam, 1977), p. 3.

[14]M. Pinard, B. Kleinmann, G. Grynberg, D. Bloch, and M. Ducloy, J. Phys. (Paris) **46**, 149 (1985).

[15]D. G. Steel and R. C. Lind, Opt. Lett. **6**, 587 (1981).

[16]M. Pinard, P. Verkerk, and G. Grynberg, Opt. Lett. **9**, 399 (1984).

[17]F. Biraben, Opt. Commun. **29**, 353 (1979); F. Biraben and P. Labastie, *ibid.* **41**, 49 (1982).

[18]P. Verkerk, M. Pinard, and G. Grynberg, Opt. Commun. **55**, 215 (1985).

[19]P. Verkerk, Ph.D. dissertation, University of Paris, Paris, 1985.

[20]M. Pinard, P. Verkerk, and G. Grynberg (unpublished).

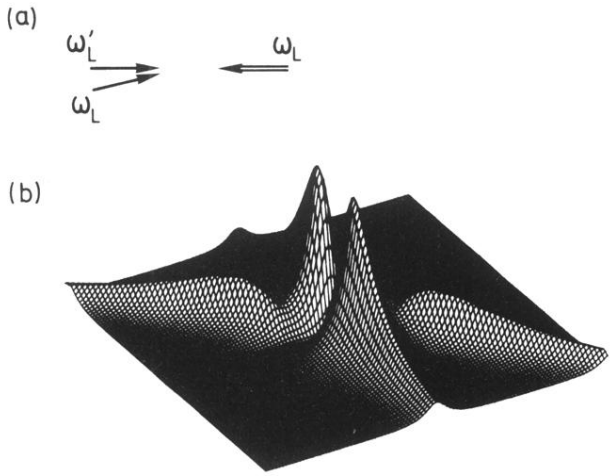

FIG. 10. (a) Four-wave mixing emission in the case when the frequency ω_L of the weak pump beam is different from the frequency ω_L of the intense pump and of the probe. Variation of I_{pc} vs δ and δ'. (b) The surface is obtained in the infinite-Doppler-width limit.

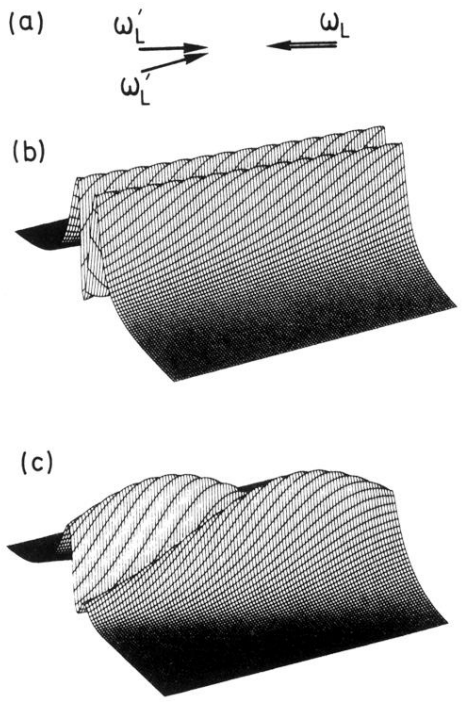

FIG. 7. (a) Four-wave mixing emission in the case of weak beams of same frequency. Variation of I_{pc} vs δ and δ'. The surfaces are calculated (b) in the infinite-Doppler-width limit and (c) in the case $\Omega_1/ku = 0.1$.

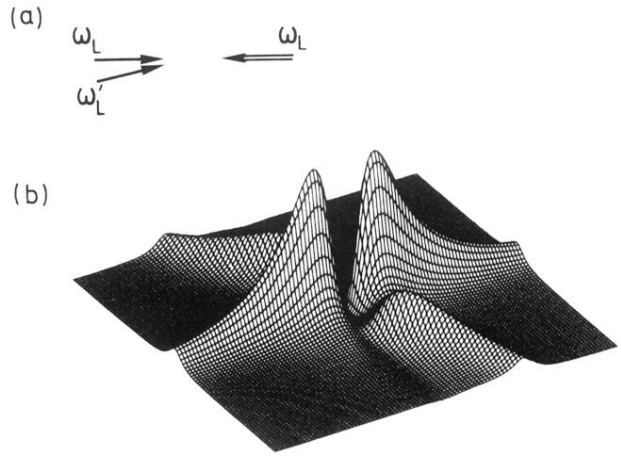

FIG. 9. (a) Four-wave-mixing emission in the case of two pump beams of same frequency. Variation of I_{pc} versus δ and δ'. (b) The surface is obtained in the infinite-Doppler-width limit.